The NOAH HSQC-COSY module revisited: a theoretical and practical comparison of pulse sequences

Jonathan R. J. Yong,[1] Ēriks Kupče,[2] Tim D. W. Claridge[1,*]

[1] *Chemistry Research Laboratory, Department of Chemistry, University of Oxford, Mansfield Road, Oxford OX1 3TA, United Kingdom*

[2] *Bruker UK Ltd, R&D, Coventry CV4 9GH, United Kingdom*

[*] `tim.claridge@chem.ox.ac.uk`

Abstract

TOC PIC GOES HERE

- Detailed discussion of HSQC-COSY implementations in NMR supersequences.

- Comparison of HSQC-COSY with HSQC-TOCSY.

- Sensitivity analyses of modules within typical NMR supersequences involving HSQC-COSY experiments.

NMR supersequences, as exemplified by the NOAH (NMR by Ordered Acquisition using ^{1}H detection) technique, are a powerful way of acquiring multiple 2D data sets in much shorter durations. This is accomplished through targeted excitation and detection of the magnetisation belonging to specific isotopologues ('magnetisation pools'). Separately, the HSQC-COSY experiment has recently seen an increase in popularity due to the high signal dispersion in the indirect dimension and the removal of ambiguity traditionally associated with HSQC-TOCSY experiments. Here, we describe how the HSQC-COSY experiment can be integrated as a 'module' within NOAH supersequences. The benefits and drawbacks of several different pulse sequence implementations are discussed, with a particular focus on how sensitivities of other modules in the same supersequence are affected.

1 Introduction

The acceleration of multidimensional NMR spectroscopy has been an extremely popular topic in recent years, with techniques ranging from ultrafast NMR[1–3] and non-uniform sampling (NUS)[4–6] to multiple-receiver technology[7–9] and reduction of recovery delays.[10–12] NOAH (NMR by Ordered Acquisition using ^{1}H detection) experiments,[13] which fall under the category of multiple-FID experiments,[14] concatenate multiple 2D experiments ('modules') into a single nested pulse sequence with elision of intermediate recovery delays. Such 'supersequences' provide up to 4× time savings compared to conventional, one-by-one acquisition of each 2D spectrum, and have gained popularity due to their versatility as well as the fact that they do not require specialised hardware.
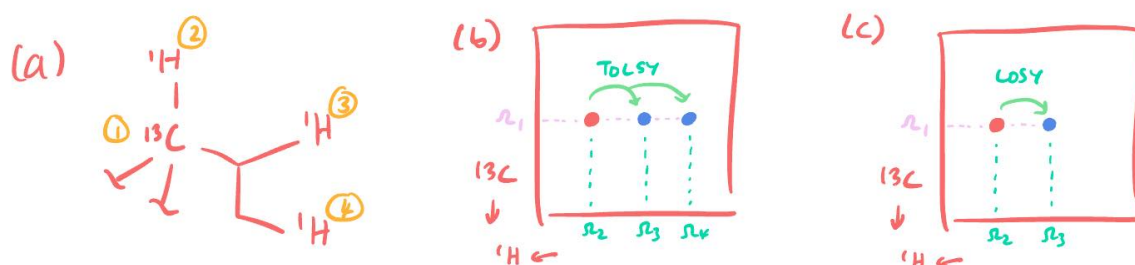

Figure 1: **(a)** A typical fragment of an organic molecule, with one ^{13}C and three ^{1}H spins. **(b)** The corresponding HSQC-TOCSY spectrum. The 'direct' peak at (Ω_1, Ω_2) is shown in red, and the 'indirect' peaks at (Ω_1, Ω_3) and (Ω_1, Ω_4) in blue: these have different signs due to an 'editing' spin echo described later in the text. **(b)** The corresponding HSQC-COSY spectrum, which is similar to the HSQC-TOCSY spectrum, except that there is only one 'indirect' peak which arises from coherence transfer over $^3J_{HH}$.

Virtually all of the most commonly used 2D experiments have been adapted for use within NOAH supersequences, as neatly listed on the GENESIS website.[15] In particular, we have previously described the implementation of the HSQC-TOCSY module in NOAH supersequences.[16] The HSQC-TOCSY experiment is extremely information-rich, providing both 'direct' responses which arise from directly bonded ^{13}C–^{1}H pairs, and 'indirect' responses from protons in the same spin system as those bound to ^{13}C (Figures 1a and 1b) This is essentially the same information as in separate HSQC and TOCSY spectra, but with the additional benefit that the TOCSY signals are dispersed more widely across the ^{13}C indirect dimension: this serves to greatly reduce the possibility of overlap and thus increase interpretability.

One downside of the HSQC-TOCSY is the largely indiscriminate transfer of magnetisation effected by the isotropic mixing block, which means that it is difficult to determine with certainty the number of bonds separating the ^{13}C and ^{1}H resonances in the 'indirect' responses. A direct method of overcoming this is to instead record an HSQC-COSY spectrum, where the 'indirect'

responses arise only from single-step coherence transfer between directly coupled ^1H–^1H pairs (Figure 1c). Experiments of this kind date back almost two decades, including the celebrated H2BC experiment,[17,18] and later 2BOB/H2OBC[19] and HMQC-COSY.[20] The 2BOB experiment in particular has previously been incorporated in NOAH supersequences.[21] Since then, the HSQC-CLIP-COSY[22,23] has emerged as a modern and improved experiment for this purpose: it provides pure absorption-mode lineshapes and does not suffer from amplitude modulation due to proton–proton couplings, a downside of the constant-time technique used in some of its predecessors.

Although the HSQC-CLIP-COSY performs admirably as a standalone experiment, the requirements for NOAH supersequences are more stringent: in particular, any HSQC-COSY module should—ideally—preserve unused magnetisation for later modules. The most important example of this is magnetisation of all protons not directly bound to ^{13}C (denoted[16,24] '$^1\text{H}^{!C}$'). The HSQC-COSY module does not use this 'magnetisation pool', and if it returns this magnetisation to the equilibrium $+z$ position, it can be sampled in a homonuclear module later in the supersequence. Another key feature of the NOAH HSQC-TOCSY module is the fact that it allows for variable excitation of ^{13}C–bound proton magnetisation (denoted '$^1\text{H}^{C}$'), meaning that a portion of it can be saved for a later heteronuclear module (e.g. an HSQC). This feature was directly inspired by the ASAP-HMQC[10] and HSQC[11,12,25,26] sequences, which store partial $^1\text{H}^{C}$ magnetisation for subsequent t_1 increments instead of different modules. We should therefore like any implementation of the HSQC-COSY to also exhibit this flexibility, as it allows the user to fine-tune the sensitivities of the modules within the supersequence for maximal performance.

In this work, we evaluate three different implementations of the NOAH HSQC-COSY module against several different criteria. These pulse sequences have been very briefly described in our previous work, but in a different context of 'parallel' supersequences:[27] here we go into substantially more depth about the development, and the relative merits of, the three different HSQC-COSY forms.

2 HSQC-CLIP-COSY

The first implementation is the direct usage of the HSQC-CLIP-COSY sequence as a NOAH module (Figure 2). In this sequence, a standard HSQC experiment is supplemented with a clean in-phase (CLIP) coherence transfer block, formed from a perfect echo[29–31] and a zero-quantum filter[28] (Figure 2). The spin echo of duration 4Δ just prior to detection allows for evolution of $^1J_{\text{CH}}$, meaning that the 'direct' responses acquire a negative sign, as illustrated in Figure 1c. Because of this inversion of direct responses, additional multiplicity editing in the HSQC step would lead to confusing spectra: thus, although the pulse sequences available on GENESIS
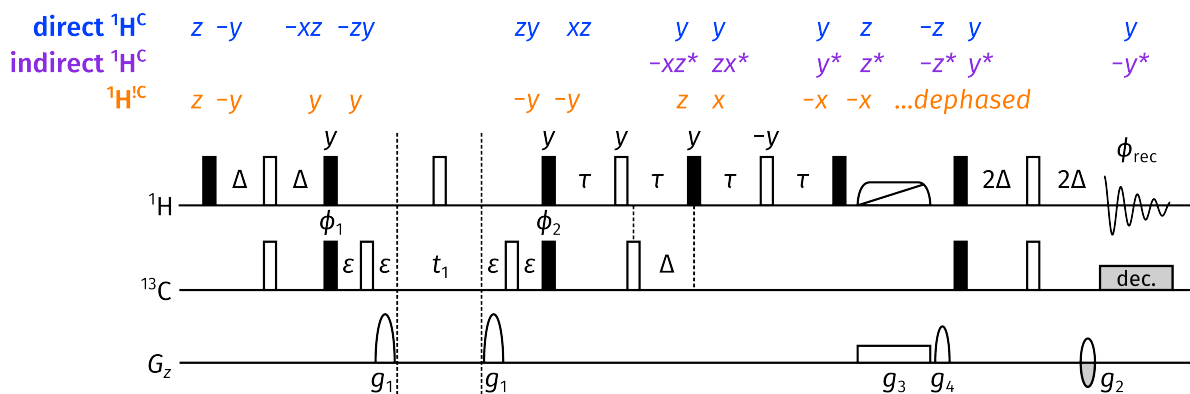
3

Figure 2: HSQC-CLIP-COSY experiment with product operator analysis for a three-spin *ISR* system, where *I* is ^{13}C, *S* is a directly bonded ^{1}H, and *R* a remote proton. Spins *I* and *S* are connected via one-bond ^{13}C–^{1}H scalar coupling, and *S* and *R* via a (typically three-bond) ^{1}H–^{1}H scalar coupling. Product operator analysis is provided for three relevant magnetisation pools: the 'direct ^{1}H^C' HSQC-type peaks, the 'indirect ^{1}H^C' responses which arise from coherence transfer from *S* to *R* in the perfect echo block, and the '^{1}H$^{!C}$' bulk magnetisation which we seek to preserve. Single-letter terms are shorthand for magnetisation on spin *S* (for example, *x* represents S_x); double-element terms to magnetisation on spins *I* and *S* (for example, *xz* is $2I_xS_z$). Letters with asterisks refer to magnetisation on the remote spin *R*; thus, for example, y^* means R_y, and xz^* means $2I_xR_z$. Solid bars are 90° pulses and empty bars 180° pulses; the rounded trapezoid and line represent an adiabatic inversion pulse. All pulses are applied along the +*x*-axis unless otherwise specified; the symbolic pulse phases are $\phi_1 = (x, -x)$; $\phi_2 = (x, x, -x, -x)$; and $\phi_{rec} = (x, -x, -x, x)$. Pulsed field gradient amplitudes are $g_1 = 37.10$ G cm^{-1} and $g_2 = 18.66$ G cm^{-1}. The gradient g_3 should be calibrated as per Thrippleton et al.;[28] g_4 is a purge gradient with arbitrary amplitude. The delays Δ and τ are chosen to be $1/(4 \cdot \,^1J_{CH})$ and $1/(4 \cdot \sum\,^nJ_{HH})$; typically, $^1J_{CH}$ and $\sum\,^nJ_{HH}$ are respectively set as 145 Hz and 30 Hz, leading to values of $\Delta = 1.72$ ms and $\tau = 8.33$ ms. ε is the minimum time required for a pulsed field gradient plus a gradient recovery delay.

do allow for multiplicity editing via an optional flag, they are omitted in the discussion which follows.

The main benefit of the HSQC-CLIP-COSY sequence is the pure absorption-mode lineshapes yielded by the CLIP transfer (Figure 3a). In this regard, it is the clear winner of all the sequences explored in this paper, as all the others generate a mixture of in-phase absorption and antiphase dispersion lineshapes. However, this comes at a price: there is no way for this sequence to preserve any magnetisation for later modules, as the product operator analysis shows: all unused magnetisation is dephased by the end of the sequence.

It is reasonable to question whether minor adjustments can be made to the pulse sequence to render it NOAH-compatible, as has previously been done for modules such as HMBC[21,32] and sensitivity-enhanced HSQC.[16,33] However, unfortunately, the CLIP element is wholly incompatible with preservation of unused magnetisation. Specifically, the zero-quantum filter dephases any magnetisation that is not along ±*z* at this time. However, if the 'bulk' ^{1}H$^{!C}$ magnetisation were to be placed along ±*z*, there would be no way to later differentiate it from the 'indirect
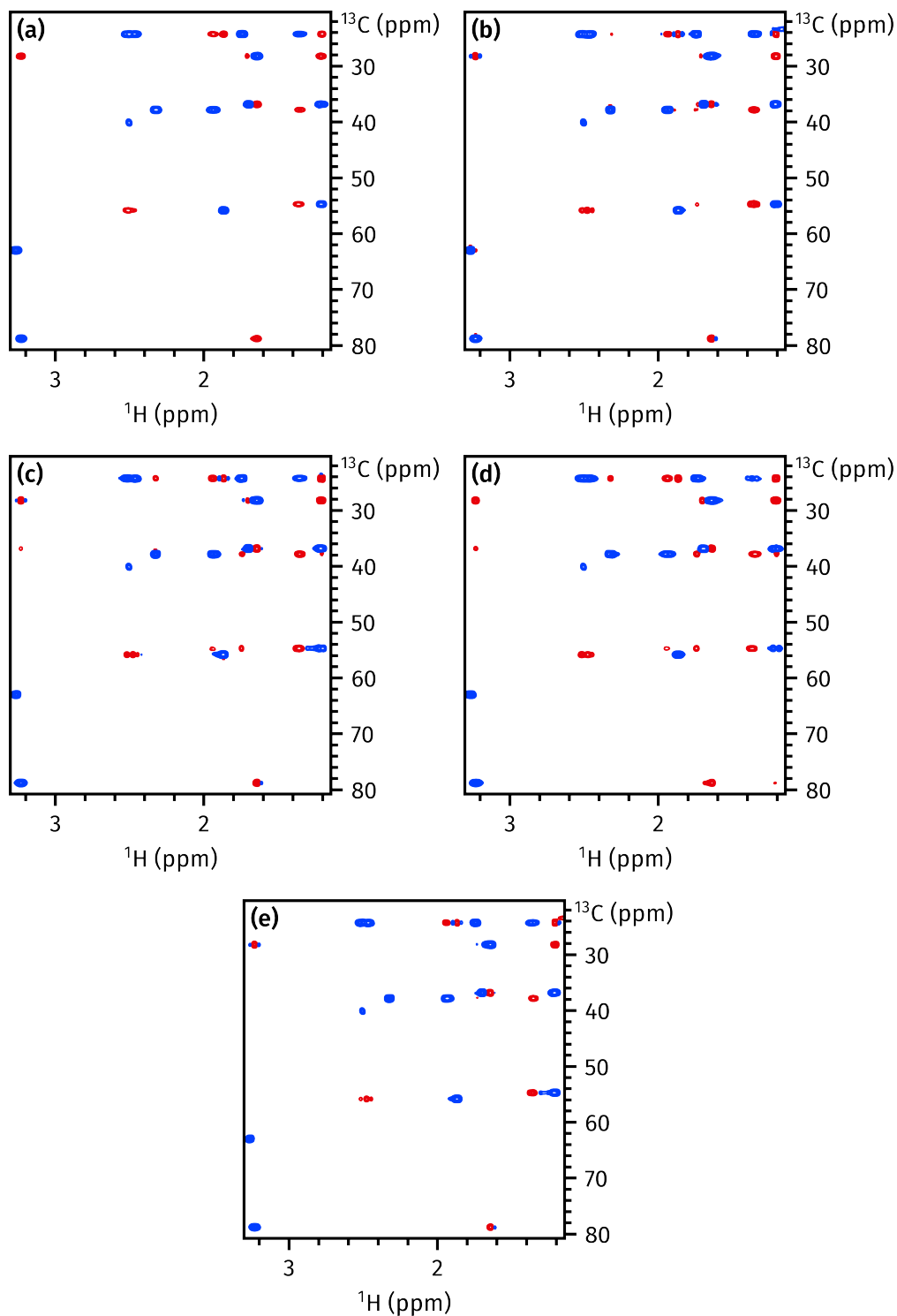
Figure 3: HSQC-COSY and HSQC-TOCSY spectra, taken from (respectively) NOAH-3 $S^C SC^c$ and NOAH-3 $S^T SC^c$ experiments. **(a)** HSQC-CLIP-COSY. **(b)** DSE HSQC-COSY. **(c)** TSE HSQC-COSY without suppression of relay artefacts (described in the text). **(d)** HSQC-TOCSY with 10 ms mixing time. **(e)** TSE HSQC-COSY with suppression of relay artefacts. Spectra were obtained on a 700 MHz Bruker AV III equipped with a TCI H/C/N cryoprobe; the sample used was 40 mM andrographolide in DMSO-d_6. 256 t_1 increments were used, with 2 transients per t_1 increment. All spectra are plotted with the same contour levels.
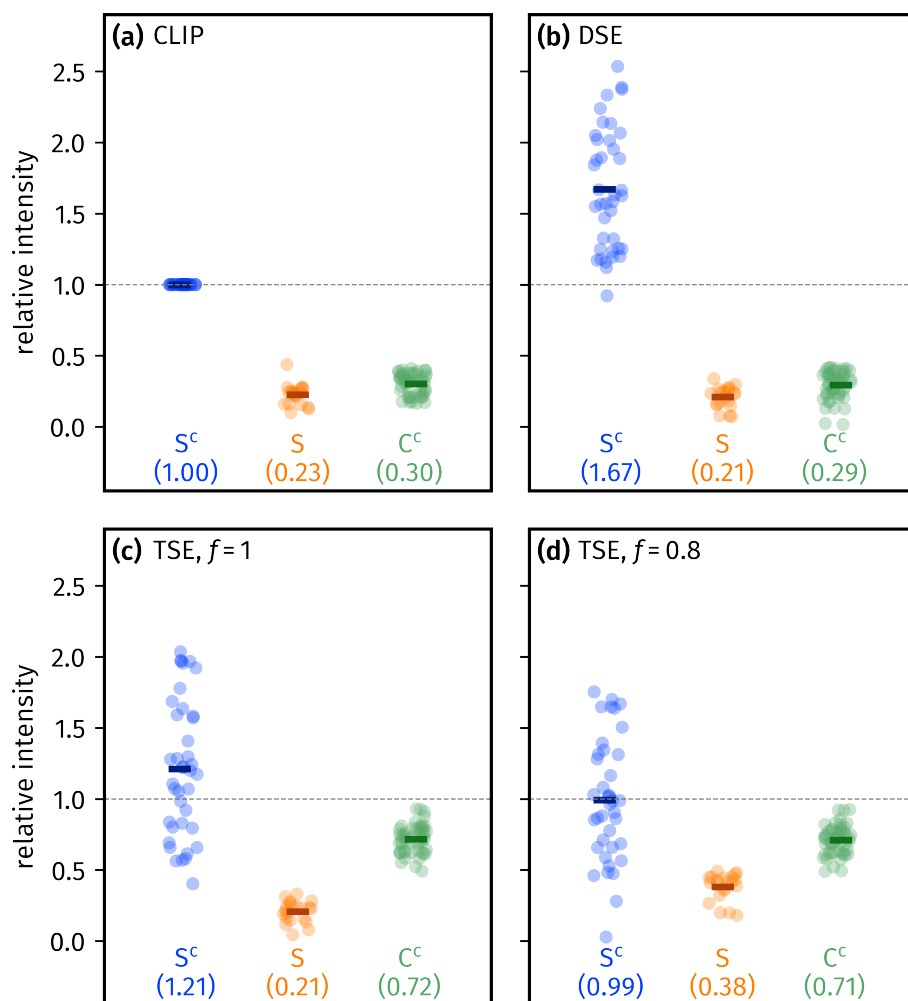
Figure 4: (Insert schematic of NOAH supersequence.) Sensitivity comparisons for all three modules in NOAH-3 $S^C SC^c$ (HSQC-COSY + HSQC + CLIP-COSY) supersequences, using a variety of implementations for the HSQC-COSY module. Peak intensities of the first module are measured relative to the HSQC-CLIP-COSY module itself (the leftmost column in (a)); whereas peak intensities of the HSQC and CLIP-COSY modules are measured relative to a separate, reference, NOAH-2 SC^c experiment. Numbers in parentheses indicate averages over all peaks. **(a)** HSQC-CLIP-COSY. **(b)** DSE HSQC-COSY. **(c)** TSE HSQC-COSY, acquired with $f = 1$. **(d)** TSE HSQC-COSY, acquired with $f = 0.8$. Spectra were obtained on a 700 MHz Bruker AV III equipped with a TCI H/C/N cryoprobe; the sample used was 40 mM andrographolide in DMSO-d_6.

^{1}H^C' magnetisation, since neither of these evolve under $^1J_{CH}$. Similar considerations preclude the possibility of variable ^{1}H^C excitation: if we had a portion of unused ^{1}H^C magnetisation that was intended to be stored for a subsequent module, this would have to be placed along the z-axis during the zero-quantum filter, but it cannot then be disentangled from the 'direct ^{1}H^C' component which we do intend to detect.

A typical example of a NOAH supersequence featuring the HSQC-COSY module is a NOAH-3 $S^C SC^c$ supersequence (FIG 4A; S^C = HSQC-COSY, S = HSQC, and C^c = CLIP-COSY). From a practical perspective, the HSQC module can be configured to include, for example, multiplicity

editing or coupling in F_2, which provides additional information not present in the HSQC-COSY.

In the present work, however, this supersequence is chosen to illustrate the effect of varying the HSQC-COSY implementation on downstream modules. Because the HSQC-CLIP-COSY consumes all $^1\mathrm{H}^\mathrm{C}$ and $^1\mathrm{H}^\mathrm{!C}$ magnetisation, both the HSQC and CLIP-COSY which come after it only sample magnetisation that has recovered during the acquisition periods interspersed between modules. Thus, both of these modules have substantially reduced sensitivity (Figure 4a) when compared against a NOAH-2 SC$^\mathrm{c}$ supersequence (i.e., the same supersequence but with the HSQC-COSY removed).
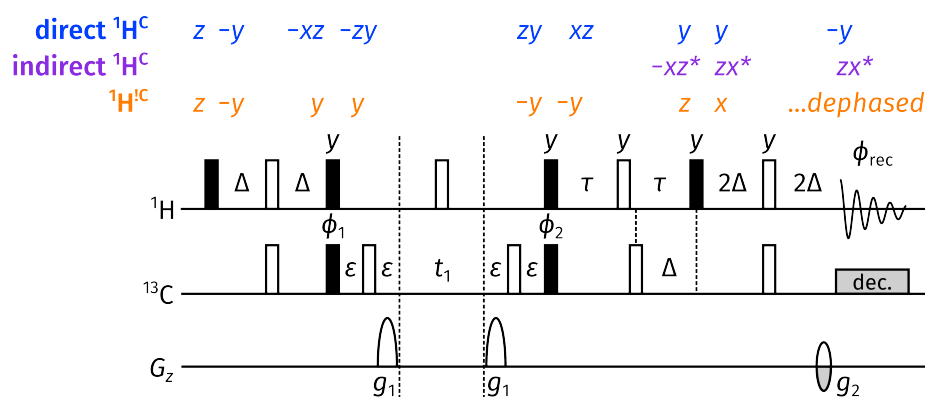
3 Double spin echo HSQC-COSY

Figure 5: 'Double spin echo' HSQC-COSY experiment; all symbols have the same meaning as in Figure 2.

The purpose of the CLIP element in the HSQC-CLIP-COSY is to effect coherence transfer from one proton to another proton coupled to it. However, given that this CLIP element makes it impossible to preserve unused magnetisation, it is worth considering what happens when this is replaced with the simplest pulse sequence element for coherence transfer—namely, a spin echo followed by a 90° pulse. This simplification results in the 'double spin echo' (DSE) HSQC-COSY, so-named because it has two spin echoes after the t_1 period (Figure 5).

The removal of the CLIP element leads to mixed lineshapes in this experiment, where the direct responses are (mostly) in-phase absorption, and the indirect responses (mostly) antiphase dispersion. This is clearly visible in the spectrum (Figure 3b): the antiphase dispersion components are visible as 'wings' of opposite sign which flank each peak. On the other hand, because the antiphase magnetisation generated during the spin echo is not purged, the DSE HSQC-COSY sequence provides the greatest sensitivity of all the HSQC-COSY implementations here: for the sample used here, it yielded (on average) a 60% increase in sensitivity compared to the HSQC-CLIP-COSY. Unfortunately, as before, the DSE experiment does not preserve bulk magnetisation; it is

also incompatible with partial $^1\text{H}^C$ excitation. Thus, the sensitivities of the subsequent modules in the NOAH-3 S^CSC^c supersequence remain very low (Figure 4b), and (accounting for noise) are identical to those seen previously with the HSQC-CLIP-COSY.
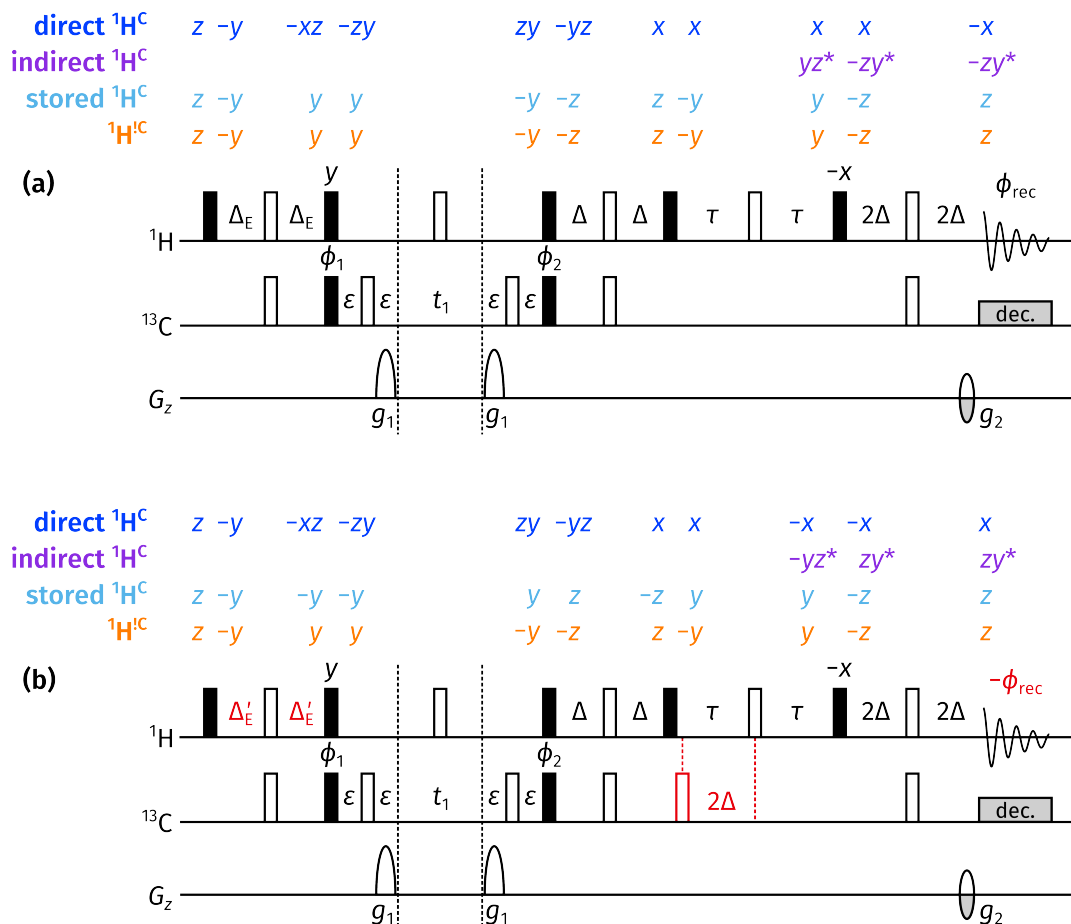
4 Triple spin echo HSQC-COSY

Figure 6: 'Triple spin echo' (TSE) HSQC-COSY experiment. **(a)** The first part of the experiment; this can be used on its own, but leads to spurious 'relayed' peaks arising via coherence transfer over two scalar couplings. The initial INEPT delay Δ_E can be adjusted so as to excite only a portion of the $^1\text{H}^C$ magnetisation pool: to excite a fraction $f \in [0, 1]$ of this magnetisation, Δ_E should be set to $(2\Delta \arcsin f)/\pi$. **(b)** The second part of the experiment; co-adding this dataset with the first part leads to suppression of the relayed peaks. Differences from (a) are highlighted in red: in particular, the value of Δ'_E should be $(2\Delta(\pi - \arcsin f))/\pi$. All other symbols have the same meaning as in Figure 2.

As shown above, neither of the two HSQC-COSY implementations above (CLIP or DSE) can successfully preserve unused magnetisation. The triple spin echo (TSE) HSQC-COSY was introduced to remedy this problem. We first consider only the 'basic', first part of the TSE HSQC-COSY (Figure 6a). This pulse sequence differs from the DSE HSQC-COSY by the splitting up of the first of the two spin echoes after t_1 into two separate spin echoes: one of duration 2Δ for

$^1J_{CH}$ refocusing, and one of duration 2τ for $^nJ_{HH}$ evolution. This not only leads to preservation of the bulk $^1H^{!C}$ magnetisation, but also enables partial $^1H^C$ excitation by shortening the delay Δ in the initial INEPT step to Δ_E. The product operators immediately after the second Δ_E delay are $\cos(2\pi J_{IS}\Delta_E)I_y - \sin(2\pi J_{IS}\Delta_E)2I_xS_z$; thus, if we want to excite a proportion f of $^1H^C$ magnetisation ($0 \leq f \leq 1$), we should set

$$f = \sin(2\pi J_{IS}\Delta_E) \implies \Delta_E = \arcsin f/(2\pi J_{IS}),$$

and since $\Delta = 1/(4J_{IS})$, we have that $\Delta_E = (2\Delta \arcsin f)/\pi$. This is identical to that previously described for the NOAH HSQC-TOCSY module[16] (although a factor of $2/\pi$ was erroneously omitted there).

While this sequence exhibits the desired behaviour in terms of magnetisation preservation, the introduction of one extra spin echo leads to the possibility of two-step coherence transfer through successive ^1H–^1H couplings and thus spurious peaks. In particular, the intensity of this unwanted transfer pathway is proportional to the extent to which J_{SR} evolves during the first spin echo after t_1: therefore, these 'relay' artefacts are especially prominent for large magnitudes of J_{SR}, such as ^2J or axial–axial ^3J. This is seen clearly in the resulting spectrum (Figure 3c): a number of extra peaks are visible compared to the CLIP and DSE HSQC-COSY implementations. Indeed, this naive implementation of the TSE HSQC-COSY very much resembles a HSQC-TOCSY acquired with a short mixing time (Figure 3d), which defeats the purpose of the HSQC-COSY experiment.

This drawback, however, can be elegantly addressed by the introduction of a second experiment (Figure 6b). The most obvious difference here is the addition of a single ^{13}C 180° pulse, highlighted in red. This addition causes $^1J_{CH}$ to evolve for a total duration of 4Δ during the 2τ spin echo, causing any magnetisation of ^{13}C–bound protons to be inverted. Conversely, magnetisation which has already undergone coherence transfer to a remote proton during the preceding spin echo is not affected. Thus, the effect is to invert the desired signal, while leaving the relay artefacts untouched. Subtracting this second dataset from the first (or equivalently, as is done here, inverting the receiver phase on the second and then adding them together) leads to suppression of the relay artefacts.

A more subtle point is that the insertion of an extra 180° pulse also causes any unexcited (i.e., stored) $^1H^C$ magnetisation to be inverted. In order to ensure that this is returned to $+z$ at the end of the sequence, instead of $-z$, a slight adjustment must also be made to the INEPT delay for variable excitation: instead of being shortened, it must be lengthened to a value of $\Delta'_E = (2\Delta(\pi - \arcsin f))/\pi$, where as before f is the fraction of $^1H^C$ magnetisation to be excited.

In the pulse sequences provided, the two versions of the TSE sequence are executed on alternate transients: therefore, there is no need to separately run two different experiments and later add

the individual spectra. However, it does require that an even number of transients are used. In practice, the suppression of the relay artefacts works extremely well, as shown in the resulting spectrum (Figure 3e): the peaks correspond exactly to those in the CLIP-COSY. In terms of the sensitivity of the HSQC-COSY itself, this version comes in the middle: due to the slightly greater length of the sequence compared to the DSE version, there is a small reduction in sensitivity, but it remains more sensitive than the HSQC-CLIP-COSY (Figure 4c). (The sensitivity of the 'naive' TSE HSQC-COSY is not compared here, since that experiment has spurious increases in peak height due to multi-step transfer pathways.)

The effect on the downstream modules, however, is where the TSE version truly shines. When acquired with $f = 1$ (Figure 4c), no residual $^1\mathrm{H}^C$ magnetisation is saved for the HSQC which comes after it: therefore, the sensitivity of the HSQC module is unchanged from previous examples. On the other hand, the CLIP-COSY module, which uses $^1\mathrm{H}^{!C}$ magnetisation, retains a large proportion of its sensitivity. While this sensitivity boost is less relevant for the CLIP-COSY module, which already has a high intrinsic sensitivity, it is substantially more important for other homonuclear modules which may occupy the same spot in a supersequence, such as NOESY or PSYCHE. (The remaining losses in this module likely come from the evolution of $^n J_{\mathrm{HH}}$ during the 2τ spin echo, during which $^1\mathrm{H}^{!C}$ magnetisation is placed in the transverse plane.)

The implementation of variable excitation further allows the user to divert more $^1\mathrm{H}^C$ magnetisation towards the HSQC module, in order to balance the sensitivities of the HSQC-COSY and HSQC. As an example, we recorded the same supersequence but with $f = 0.8$ (Figure 4d): this has no impact on the CLIP-COSY sensitivity but leads to an almost twofold increase in the HSQC sensitivity.

5   Supersequences with the HMBC

The relative merits of the three HSQC-COSY implementations described thus far are summarised in Table 1. Clearly, while the TSE HSQC-COSY cleaves most to the ideal concept of a NOAH module (and is therefore recommended as the default in the GENESIS website), there are tradeoffs involved in choosing any of these. We mention here a further consideration which may influence the user's choice, namely, the addition of the HMBC module to the beginning of a supersequence, which dephases all unused $^1\mathrm{H}^{!C}$ magnetisation: therefore, in a supersequence which begins with the HMBC module, the fact that the TSE HSQC-COSY preseves $^1\mathrm{H}^{!C}$ magnetisation is less relevant.

This is quantified in Figure 7, which provides the same sensitivity comparisons as before, but using a NOAH-4 BS^{C}SC^c supersequence (B = HMBC) instead. The 'reference' spectra used to calculate relative sensitivities are the same as that in Figure 4. Thus, any deviations between the

HSQC-COSY method	Pros and cons
CLIP	+ Pure absorption lineshapes − Low sensitivity − Dephases all unused magnetisation
DSE	− Mixed-phase lineshapes + High sensitivity − Dephases all unused magnetisation
TSE	− Mixed-phase lineshapes + Preserves $^1\mathrm{H}^{!C}$ magnetisation + Compatible with variable $^1\mathrm{H}^C$ excitation − Requires an even number of transients

Table 1: Comparison of NOAH HSQC-COSY modules.

two graphs derive solely from the addition of the HMBC module.

Compared to Figure 4, there is a uniform and slight drop in the sensitivity of the HSQC-COSY modules. This is due to the slightly imperfect preservation of $^1\mathrm{H}^C$ magnetisation by the HMBC module. The more relevant module to compare, though, is the CLIP-COSY. The TSE HSQC-COSY still outperforms the other implementations because the $^1\mathrm{H}^{!C}$ magnetisation pool has three successive acquisition periods during which it can recover, as compared to two for the other implementations. However, this advantage is greatly narrowed: the CLIP-COSY now only has 40% of its original sensitivity in Figures 7c and 7d, down from 70% in Figures 4c and 4d.

6 Conclusion

In this work, we have described in depth how the HSQC-COSY experiment may be incorporated in NOAH supersequences. Three different versions of the HSQC-COSY module were analysed, from both a theoretical perspective (using product operator analysis) as well as a practical one (using sensitivity comparisons of both NOAH-3 $S^C SC^c$ and NOAH-4 $BS^C SC^c$ supersequences). All of these modules are available on the GENESIS website (https://nmr-genesis.co.uk): the default is set to the TSE HSQC-COSY. While we believe that this is most likely to cater to the average user's needs, it is also possible for users to individually select their preferred implementation through the 'developer mode' option, where the CLIP, DSE, and TSE options are respectively labelled as `C_HSQCC_CLIP`, `C_HSQCC_DSE`, and `CI_HSQCC`. It is our hope that the exposition provided here will allow users to come to an informed decision based on their needs, and thus reap the maximum benefit from any NOAH supersequence featuring the HSQC-COSY module.
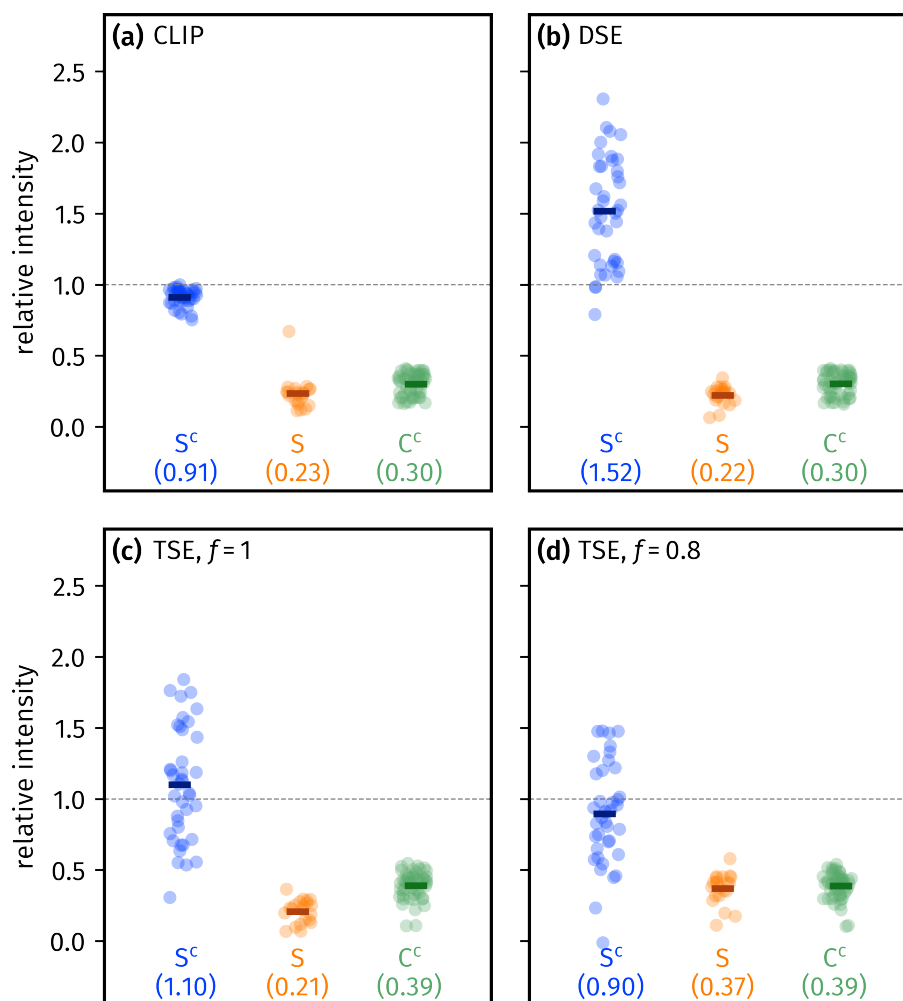
Figure 7: Sensitivity comparisons for the three last modules in NOAH-4 $BS^C SC^c$ supersequences, using different implementations of the HSQC-COSY module within. Peak intensities are relative to the HSQC-CLIP-COSY module from a NOAH-3 $S^C SC^c$ supersequence, and HSQC and CLIP-COSY spectra from a NOAH-2 SC^c experiment (these are the same reference spectra as used in Figure 4). Numbers in parentheses indicate averages over all peaks. **(a)** HSQC-CLIP-COSY. **(b)** DSE HSQC-COSY. **(c)** TSE HSQC-COSY, acquired with $f = 1$. **(d)** TSE HSQC-COSY, acquired with $f = 0.8$. Spectra were obtained on a 700 MHz Bruker AV III equipped with a TCI H/C/N cryoprobe; the sample used was 40 mM andrographolide in DMSO-d_6.

Acknowledgements

References

(1) Frydman, L.; Scherf, T.; Lupulescu, A. The acquisition of multidimensional NMR spectra within a single scan. *Proc. Natl. Acad. Sci. U. S. A.* **2002**, *99*, 15858–15862, DOI: 10.1073/pnas.252644399.

(2) Pelupessy, P. Adiabatic Single Scan Two-Dimensional NMR Spectrocopy. *J. Am. Chem. Soc.* **2003**, *125*, 12345–12350, DOI: 10.1021/ja034958g.

(3) Frydman, L.; Lupulescu, A.; Scherf, T. Principles and Features of Single-Scan Two-Dimensional NMR Spectroscopy. *J. Am. Chem. Soc.* **2003**, *125*, 9204–9217, DOI: 10.1021/ja030055b.

(4) Kazimierczuk, K.; Stanek, J.; Zawadzka-Kazimierczuk, A.; Koźmiński, W. Random sampling in multidimensional NMR spectroscopy. *Prog. Nucl. Magn. Reson. Spectrosc.* **2010**, *57*, 420–434, DOI: 10.1016/j.pnmrs.2010.07.002.

(5) Mobli, M.; Hoch, J. C. Nonuniform sampling and non-Fourier signal processing methods in multidimensional NMR. *Prog. Nucl. Magn. Reson. Spectrosc.* **2014**, *83*, 21–41, DOI: 10.1016/j.pnmrs.2014.09.002.

(6) Kazimierczuk, K.; Orekhov, V. Non-uniform sampling: post-Fourier era of NMR data collection and processing. *Magn. Reson. Chem.* **2015**, *53*, 921–926, DOI: 10.1002/mrc.4284.

(7) Kupče, Ē.; Freeman, R.; John, B. K. Parallel Acquisition of Two-Dimensional NMR Spectra of Several Nuclear Species. *J. Am. Chem. Soc.* **2006**, *128*, 9606–9607, DOI: 10.1021/ja0634876.

(8) Kupče, Ē.; Freeman, R. Molecular Structure from a Single NMR Experiment. *J. Am. Chem. Soc.* **2008**, *130*, 10788–10792, DOI: 10.1021/ja8036492.

(9) Kovacs, H.; Kupče, Ē. Parallel NMR spectroscopy with simultaneous detection of ^{1}H and ^{19}F nuclei. *Magn. Reson. Chem.* **2016**, *54*, 544–560, DOI: 10.1002/mrc.4428.

(10) Kupče, Ē.; Freeman, R. Fast multidimensional NMR by polarization sharing. *Magn. Reson. Chem.* **2007**, *45*, 2–4, DOI: 10.1002/mrc.1931.

(11) Schulze-Sünninghausen, D.; Becker, J.; Luy, B. Rapid Heteronuclear Single Quantum Correlation NMR Spectra at Natural Abundance. *J. Am. Chem. Soc.* **2014**, *136*, 1242–1245, DOI: 10.1021/ja411588d.

(12) Becker, J.; Koos, M. R. M.; Schulze-Sünninghausen, D.; Luy, B. ASAP-HSQC-TOCSY for fast spin system identification and extraction of long-range couplings. *J. Magn. Reson.* **2019**, *300*, 76–83, DOI: 10.1016/j.jmr.2018.12.021.

(13) Kupče, Ē.; Claridge, T. D. W. NOAH: NMR Supersequences for Small Molecule Analysis and Structure Elucidation. *Angew. Chem. Int. Ed.* **2017**, *56*, 11779–11783, DOI: 10.1002/anie.201705506.

(14) Yong, J. R. J.; Kupče, Ē.; Claridge, T. D. W. In *Fast 2D solution-state NMR: concepts and applications*, Giraudeau, P., Dumez, J.-N., Eds.; Royal Society of Chemistry: London, UK, 2023, DOI: 10.1039/BK9781839168062-00084.

(15) Yong, J. R. J.; Kupče, Ē.; Claridge, T. D. W. Modular Pulse Program Generation for NMR Supersequences. *Anal. Chem.* **2022**, *94*, 2271–2278, DOI: 10.1021/acs.analchem.1c04964.

(16) Yong, J. R. J.; Hansen, A. L.; Kupče, Ē.; Claridge, T. D. W. Increasing sensitivity and versatility in NMR supersequences with new HSQC-based modules. *J. Magn. Reson.* **2021**, *329*, 107027, DOI: `10.1016/j.jmr.2021.107027`.

(17) Nyberg, N. T.; Duus, J. Ø.; Sørensen, O. W. Heteronuclear Two-Bond Correlation: Suppressing Heteronuclear Three-Bond or Higher NMR Correlations while Enhancing Two-Bond Correlations Even for Vanishing $^2J_{CH}$. *J. Am. Chem. Soc.* **2005**, *127*, 6154–6155, DOI: `10.1021/ja050878w`.

(18) Nyberg, N. T.; Duus, J. Ø.; Sørensen, O. W. Editing of H2BC NMR spectra. *Magn. Reson. Chem.* **2005**, *43*, 971–974, DOI: `10.1002/mrc.1698`.

(19) Kupče, Ē.; Sørensen, O. W. 2BOB - extracting an H2BC and an HSQC-type spectrum from the same data set, and H2OBC - a fast experiment delineating the protonated ^{13}C backbone. *Magn. Reson. Chem.* **2017**, *55*, 515–518, DOI: `10.1002/mrc.4584`.

(20) Hu, K.; Westler, W. M.; Markley, J. L. Two-dimensional concurrent HMQC-COSY as an approach for small molecule chemical shift assignment and compound identification. *J. Biomol. NMR* **2011**, *49*, 291–296, DOI: `10.1007/s10858-011-9494-4`.

(21) Kupče, Ē.; Claridge, T. D. W. New NOAH modules for structure elucidation at natural isotopic abundance. *J. Magn. Reson.* **2019**, *307*, 106568, DOI: `10.1016/j.jmr.2019.106568`.

(22) Gyöngyösi, T.; Timári, I.; Haller, J.; Koos, M. R. M.; Luy, B.; Kövér, K. E. Boosting the NMR Assignment of Carbohydrates with Clean In-Phase Correlation Experiments. *ChemPlusChem* **2018**, *83*, 53–60, DOI: `10.1002/cplu.201700452`.

(23) Gyöngyösi, T.; Timári, I.; Sinnaeve, D.; Luy, B.; Kövér, K. E. Expedited Nuclear Magnetic Resonance Assignment of Small- to Medium-Sized Molecules with Improved HSQC-CLIP-COSY Experiments. *Anal. Chem.* **2021**, *93*, 3096–3102, DOI: `10.1021/acs.analchem.0c04124`.

(24) Orts, J.; Gossert, A. D. Structure determination of protein-ligand complexes by NMR in solution. *Methods* **2018**, *138-139*, 3–25, DOI: `10.1016/j.ymeth.2018.01.019`.

(25) Schulze-Sünninghausen, D.; Becker, J.; Koos, M. R. M.; Luy, B. Improvements, extensions, and practical aspects of rapid ASAP-HSQC and ALSOFAST-HSQC pulse sequences for studying small molecules at natural abundance. *J. Magn. Reson.* **2017**, *281*, 151–161, DOI: `10.1016/j.jmr.2017.05.012`.

(26) Koos, M. R. M.; Luy, B. Polarization recovery during ASAP and SOFAST/ALSOFAST-type experiments. *J. Magn. Reson.* **2019**, *300*, 61–75, DOI: `10.1016/j.jmr.2018.12.014`.

(27) Kupče, Ē.; Yong, J. R. J.; Widmalm, G.; Claridge, T. D. W. Parallel NMR Supersequences: Ten Spectra in a Single Measurement. *JACS Au* **2021**, *1*, 1892–1897, DOI: `10.1021/jacsau.1c00423`.

(28) Thrippleton, M. J.; Keeler, J. Elimination of Zero-Quantum Interference in Two-Dimensional NMR Spectra. *Angew. Chem., Int. Ed.* **2003**, *42*, 3938–3941, DOI: `10.1002/anie.200351947`.

(29) Aguilar, J. A.; Nilsson, M.; Bodenhausen, G.; Morris, G. A. Spin echo NMR spectra without J modulation. *Chem. Commun.* **2012**, *48*, 811–813, DOI: `10.1039/c1cc16699a`.

(30) Parella, T. Towards perfect NMR: Spin-echo versus perfect-echo building blocks. *Magn. Reson. Chem.* **2019**, *57*, 13–29, DOI: `10.1002/mrc.4776`.

(31) Koos, M. R. M.; Kummerlöwe, G.; Kaltschnee, L.; Thiele, C. M.; Luy, B. CLIP-COSY: A Clean In-Phase Experiment for the Rapid Acquisition of COSY-type Correlations. *Angew. Chem., Int. Ed.* **2016**, *55*, 7655–7659, DOI: `10.1002/anie.201510938`.

(32) Claridge, T. D. W.; Mayzel, M.; Kupče, Ē. Triplet NOAH supersequences optimised for small molecule structure characterisation. *Magn. Reson. Chem.* **2019**, *57*, 946–952, DOI: `10.1002/mrc.4887`.

(33) Hansen, A. L.; Kupče, Ē.; Li, D.-W.; Bruschweiler-Li, L.; Wang, C.; Brüschweiler, R. 2D NMR-Based Metabolomics with HSQC/TOCSY NOAH Supersequences. *Anal. Chem.* **2021**, *93*, 6112–6119, DOI: `10.1021/acs.analchem.0c05205`.

Supporting Information

for

The NOAH HSQC-COSY module revisited: a theoretical and practical comparison of pulse sequences

Jonathan R. J. Yong,[1] Ēriks Kupče,[2] Tim D. W. Claridge[1,*]

[1] *Chemistry Research Laboratory, Department of Chemistry, University of Oxford, Mansfield Road, Oxford OX1 3TA, United Kingdom*

[2] *Bruker UK Ltd, R&D, Coventry CV4 9GH, United Kingdom*

[*] `tim.claridge@chem.ox.ac.uk`

Contents

S1 Software and raw data

All processing was carried out using TopSpin 3 or 4. Plots are generated in Python 3, using the `numpy`, `scipy`, and `penguins` libraries. The raw data used for this paper, as well as all scripts required for regenerating the plots, are available on GitHub: `https://github.com/yongrenjie/hsqc-cosy-paper`.